2008 American Control Conference
Westin Seattle Hotel, Seattle, Washington, USA
June 11-13, 2008

Stack-level Validation of a Semi-Analytic Channel-to-Channel Fuel Cell Model for Two-Phase Water Distribution Boundary Value Control

B.A. McCain and J.B. Siegel and A.G. Stefanopoulou

Abstract— **A dynamic model combining analytic and numeric solutions to the partial differential equations (PDE) describing mass transport in the gas diffusion layers (GDL) of a fuel cell is verified by voltage prediction. The model estimates the effect of stack temperature changes, reactant gas concentration fluctuation, and excess liquid water (flooding) in the GDL. The semi-analytic model is more computationally efficient than a fully numeric model, and includes both anode and cathode channel dynamics enabling future boundary value control.**

I. Introduction and Motivation

Fuel cell technology holds significant promise for clean and renewable power generation for both stationary and mobile applications. Of critical importance to the efficient and long-life operation of a fuel cell system are:

- Maintaining humidity in a narrow range near water vapor saturation at the membrane while avoiding excess accumulation of liquid water in the channels (flooding).
- Keeping sufficient reactant concentration at the membrane to avoid starvation.

The time-varying constituent distributions in the anode and cathode GDLs are described by six 2^{nd} order parabolic PDEs for reactant (oxygen in the cathode and hydrogen in the anode) concentration, water vapor concentration, and liquid water volume. The electrochemical reactions on, and the mass transport through, the catalyst-covered membrane couple the anode and cathode behaviors and, together with the channel conditions, provide the time-varying boundary values for these PDEs.

Simplified models attempting to either focus on a particular model component or phenomena or to pursue a reduced form to facilitate control exist in abundance. These models contain restrictions such as single-phase water, GDL only ([1],[2]), steady-state conditions ([3]), and the common assumption of isothermal conditions. Most of these models still conclude using numeric solutions to describe the fuel cell dynamics, and though simplified and insightful, they do not quite provide the model reduction focus desired.

The water (liquid and vapor) PDEs are tightly coupled through the evaporation/condensation rate. Further, the liquid water becomes a nonlinearly distributed parameter that inhibits reactant gas and water vapor diffusion. Specifically, liquid water occupies pore space in the GDL, impedes the diffusion of reactant flow towards the membrane, and ultimately reduces the active fuel cell area [4], causing performance degradation.

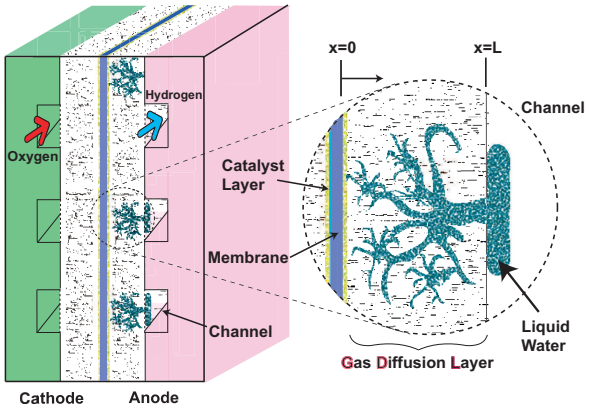

Fig. 1. Conceptual schematic showing accumulation of liquid water in the GDL and subsequent flow to the channel where reactant-blocking film is formed

Removal of accumulated liquid water is necessary to regain performance, which is typically accomplished by surging an inlet flow (e.g. anode H_2 supply). Liquid water accumulation is undesirable for performance, efficiency, and membrane durability reasons, hence it is clear that estimation and control of the liquid water distribution is critical for effective fuel cell water management. A low-order, compact model of the multi-component (reactants, water), two-phase (vapor and liquid water), spatially-distributed and dynamic behavior across the gas diffusion layer (Fig. 1) is needed.

Our goal with this work is to create a simple fuel cell water dynamics model that provides a physical understanding sufficient to enable water management using automatic control. For the dynamics within the GDL, the boundary conditions, capillary flow, and porous media transport mechanisms used herein follow close to those of [5]. We present an isothermal, one-dimensional, channel-to-channel, inlet-to-outlet, control-oriented model that combines analytic solutions for the spatial distributions of gases with a numeric solution for the liquid water, which is possible due to large time scale separation.

We demonstrate here that the model captures the cell output performance, namely the voltage during variation in temperature, current, inflows, and during flooding and drying conditions. After the verification, the model is used to investigate the feasibility of controlling water accumulation in the GDL and the channels with boundary value control.

B.A. McCain, A.G. Stefanopoulou, and J.B. Siegel (bmccain, siegeljb, and annastef@umich.edu) are with the Fuel Cell Control Laboratory, Mechanical Engineering Dept., University of Michigan.

Funding is provided from NSF-GOALI CMS-0625610 and the U.S. Dept. of Energy DE-FG02-06CH 11300.

II. Model of the Anode Gas Diffusion Layer

We proceed with a one-dimensional treatment of the anode GDL processes, letting x denote the spatial variable, with x=0 corresponding to the membrane location and x=L corresponding to the channel location, and we let t denote the time variable. The model includes channel and GDL for both anode and cathode, however details given here cover only the anode for brevity. The relationships and equations are parallel, with differences appearing only in sign, rate of reactant consumption, and the generation of water vapor on the cathode side.

The state variables are as follows:

- $c_{H_2}(x,t)$ is the hydrogen concentration (mol/m^3) at time t at a cross-section of the GDL located at x, $0 \leq x \leq L$;
- $c_{v,an}(x,t)$ is the concentration of water vapor at time t at a cross-section of GDL located at x, $0 \leq x \leq L$;
- $s(x,t)$ is the fraction of liquid water volume V_L to the total pore volume V_p, $s = \frac{V_L}{V_p}$. s is thus a concentration-like variable for the liquid water at time t, at a cross-section of GDL located at x, $0 \leq x \leq L$.

The two parabolic PDEs that govern the anode reactant and water vapor concentrations are,

$$\frac{\partial c_{H_2}}{\partial t} = \frac{\partial}{\partial x}\left(D_{H_2}(s)\frac{\partial c_{H_2}}{\partial x}\right), \tag{1}$$

$$\frac{\partial c_{v,an}}{\partial t} = \frac{\partial}{\partial x}\left(D_v(s)\frac{\partial c_{v,an}}{\partial x}\right) + r_v(c_{v,an}), \tag{2}$$

where $D_v(s)$ and $D_{H_2}(s)$ are the effective diffusivities for water vapor and hydrogen which depend on the liquid fraction, s,

$$D_j(s) = D_j\varepsilon\left(\frac{\varepsilon - 0.11}{1-0.11}\right)^{0.785}(1-s)^2, \tag{3}$$

with D_j being the binary diffusion coefficient of element j.

The evaporation rate, r_v is defined as,

$$r_v(c_{v,an}) = \begin{cases} \gamma\left(c_{v,sat} - c_{v,an}\right) & \text{for } s > 0 \\ \min\left\{0, \gamma(c_{v,sat} - c_{v,an})\right\} & \text{for } s = 0, \end{cases}$$

where γ is the volumetric condensation coefficient (s^{-1}) and $c_{v,sat}$ is the saturation vapor concentration.

The liquid accumulation is,

$$\frac{\partial s}{\partial t} = -\frac{1}{\varepsilon A_{fc}\rho_l}\frac{\partial W_l}{\partial x} - \frac{M_v}{\rho_l}r_v(c_{v,an}), \tag{4}$$

where M_j is the molar mass of constituent j. The mass flow of liquid water is driven by the gradient in capillary pressure (p_c) due to build-up of liquid water in the porous medium,

$$W_l = -\varepsilon A_{fc}\rho\frac{KK_{rl}}{\mu_l}\frac{\partial p_c}{\partial x}, \tag{5}$$

where μ_l (kg/ms) is the liquid viscosity, A_{fc} (m^2) is the fuel cell active area, and K (m^2) is the material-dependent absolute permeability. It is convenient to define the reduced liquid water saturation S as:

$$S(x,t) \triangleq \begin{cases} \frac{s(x,t) - s_{im}}{1 - s_{im}} & \text{for } s \geq s_{im}, \\ 0 & \text{for } s < s_{im}. \end{cases} \tag{6}$$

The relative liquid permeability is simply $K_{rl} = S^3$ [5].

The capillary pressure is found from a fitted 3^{rd} order polynomial (Leverett J-function) in $S(x,t)$. The condensed liquid accumulates in the GDL until it has surpassed the immobile saturation threshold (s_{im}), at which point capillary flow will carry it to an area of lower capillary pressure (toward the GDL-channel interface). The immobile water saturation s_{im} works as stiction, i.e. there is no liquid flow unless the liquid water fraction exceeds s_{im}. Using the approximation $\frac{K}{\mu_l}S^3\frac{\partial p_c}{\partial S} \approx b_1 S^{b_2}$,

$$W_l = -\varepsilon A_{fc}\rho_l b_1 S^{b_2}\frac{\partial S}{\partial x}, \tag{7}$$

where b_1 and b_2 are fitted parameters, and this approximation is only valid when $s > s_{im}$, so $W_l = 0$ when $s \leq s_{im}$.

From (4) and (7), the liquid water fraction PDE becomes,

$$\frac{\partial s}{\partial t} = \frac{\partial}{\partial x}\left(b_1 S^{b_2}\frac{\partial S}{\partial x}\right) - \frac{M_v}{\rho_l}r_v(c_{v,an}). \tag{8}$$

A. Boundary Conditions

The boundary conditions for the reactant constituents at the GDL-channel interface ($x = L$) depend on a controllable outlet valve that determines the flow out of the anode channel, the reactant inlet flow rate, and on a disturbance input which is the current density drawn from the fuel cell, $i(t)$ (A/m^2).

For $c_{H_2}(x,t)$, mixed Neumann-Dirichlet (Robin) type boundary conditions are imposed. The channel (ch) boundary condition is,

$$c_{H_2}|_{x=L} = c_{H_2,ch} = p_{H_2,ch}/\left(RT_{st}\right), \tag{9}$$

where R is the universal gas constant, T_{st} (K) is the stack temperature, and the hydrogen partial pressure in the anode channel, $p_{H_2,ch}$ (Pa), depends on the exhaust control valve, $u(t)$, as discussed in Sec. III. The membrane (mb) boundary condition is,

$$\left.\frac{\partial c_{H_2}}{\partial x}\right|_{x=0} = -\frac{N_{rct,H_2}}{D_{H_2}(s)|_{x=0}} = -\frac{1}{D_{H_2}(s)|_{x=0}}\cdot\frac{i(t)}{2F}. \tag{10}$$

For $c_{v,an}(x,t)$, similar Robin boundary conditions are imposed:

$$c_{v,an}|_{x=L} = c_{v,an,ch} = p_{v,an,ch}/\left(RT_{st}\right), \tag{11}$$

$$\left.\frac{\partial c_{v,an}}{\partial x}\right|_{x=0} = -\frac{N_{mb}}{D_v(s)}, \tag{12}$$

with the membrane water molar flux N_{mb},

$$N_{mb} = \beta_w(c_{v,ca,mb} - c_{v,an,mb}) - k_{v,0}i(t), \tag{13}$$

and β_w is a back-diffusion coefficient that depends upon the temperature, area, diffusivity, and thickness of the membrane, as well as a linear tuning parameter (discussed in [4]), and $k_{v,0}$ is a function of the membrane water content (λ_{mb}) which is calculated as in [6].

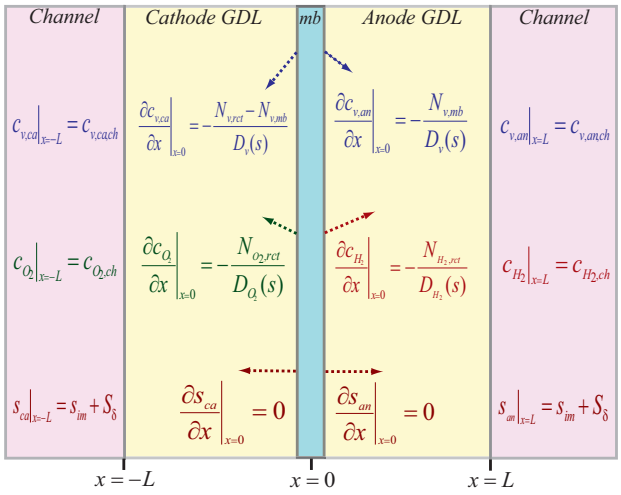

Fig. 2. Boundary conditions for anode and cathode GDL. Time-varying Neumann BC are placed at the membrane, with time-varying Dirchlet at the channels.

Finally, for $s(x,t)$, Robin boundary conditions are again imposed. Specifically, since water passing through the membrane and into the GDL is in vapor form,

$$\left.\frac{\partial s}{\partial x}\right|_{x=0} = 0. \tag{14}$$

Choosing a physically meaningful liquid water boundary condition at the GDL-channel interface has been challenging ([2],[7]) with either zero reduced liquid water saturation or zero liquid flow being typically assumed ([5],[8]). Here we consider the simplifying and convenient form of:

$$s(L,t) = s_{im} + S_\delta, \tag{15}$$

where S_δ represents the effect of the liquid water that accumulates on the GDL-channel interface, and the inclusion of S_δ essentially adds a slight resistance to flow from the GDL, but only when sufficient liquid water has accumulated to result in capillary flow into the channel. Due to a lack of a better estimate, S_δ = 0.0003 is assumed.

A graphical representation of the boundary conditions described, including appropriately similar boundary conditions imposed on the cathode GDL, is shown in Fig. 2.

III. Anode Channel Equations

We present only the anode side equations, omitting the cathode side for brevity. The anode channel H_2 and water vapor partial pressures, which represent the channel boundary conditions, are calculated from:

$$\begin{aligned} p_{H_2,ch} &= \tfrac{m_{H_2,ch} RT_{st}}{M_{H_2} V_{ch}}, \\ p_{v,an,ch} &= \min\left\{\tfrac{m_{w,ch} RT_{st}}{M_v V_{ch}}, p_{v,sat}\right\}, \\ p_{an,ch} &= p_{H_2,ch} + p_{v,an,ch}. \end{aligned} \tag{16}$$

For the anode channel calculations the governing equations for hydrogen and water are:

$$\begin{aligned} dm_{H_2,ch}/dt = &\quad (W_{H_2,in} - W_{H_2,out} + W_{H2,GDL}), \\ dm_{w,ch}/dt = &\quad (W_{w,GDL} + W_{v,in} - W_{v,out}). \end{aligned} \tag{17}$$

$W_{v,in}$=0 since the anode inlet flow is dry hydrogen, $W_{an,in}$=$W_{H_2,in}$=$k_{an,in}(p^*_{an} - p_{an,ch})$, representing a pressure-regulated anode channel at p^*_{an} which is set near the cathode pressure for membrane safety.

The constituent channel exhaust mass flow rates are found from,

$$\begin{aligned} W_{H_2,out} &= \frac{m_{H_2,an,ch}}{m_{an,ch}} W_{an,out}, \\ W_{v,out} &= W_{an,out} - W_{H_2,out}, \end{aligned} \tag{18}$$

and the anode exit flow rate to the ambient (amb) is,

$$W_{an,out} = u \cdot k_{an,out}(p_{an,ch} - p_{amb}), \tag{19}$$

and $m_{an,ch} = m_{H_2,an,ch} + p_{v,an,ch} V_{an} M_v/(RT_{st})$. $0 \le u(t) \le 1$ is for anode channel flow to remove both water and hydrogen, and u=0 represents a *dead-ended* anode arrangement, which is commonly paired with a periodic purge cycle (u=1) for water removal. For 0<u<1, it is a *flow through* anode water management system. The model verification in this work is from experimentation that employed the dead-end/purge system, though the model is applicable under both dead-end and flow through conditions.

The hydrogen and water mass flow rate from the GDL to the anode are:

$$W_{H_2,GDL} = -\varepsilon A_{fc} M_{H_2} \left(D_{H_2}(s) \frac{\partial c_{H_2}}{\partial x} \right) \Big|_{x=L}, \tag{20}$$

$$W_{w,GDL} = -\varepsilon A_{fc} \left(\rho_l b_1 S^{b_2} \frac{\partial S}{\partial x} + M_v D_v(s) \frac{\partial c_{v,an}}{\partial x} \right) \Big|_{x=L}.$$

IV. Semi-Analytic Solution

Analytic solutions for the gas and water vapor PDEs were obtained after the following observations [9]:

1) Inclusion of liquid water ratio in the diffusivity ($D_v(s)$) calculation should not be neglected, but a logical selection of a midrange value of $s = s_{im}$ results in negligible loss of accuracy.
2) Time-scale decomposition revealed that the slowest reactant gas and water vapor states have response times nearly two orders of magnitude faster than the fastest liquid water states. The water vapor states can be considered to have reached equilibrium instantaneously when addressing the liquid water PDE solution.

With the assumptions of constant diffusivities, $D_v^{s_{im}}$ and $D_{H_2}^{s_{im}}$, and extremely fast dynamic responses of the gas constituents, the steady-state solutions for vapor and hydrogen in the anode (similar for the cathode) when liquid water is present throughout the GDL ($s(x,t)$>0 $\forall x \in [0, L]$) are:

$$c_{H_2}(x) = \frac{N_{H_2 rct}}{D_{H_2}^{s_{im}}}(L - x) + c_{H_2,ch}, \tag{21}$$

$$c_{v,an}(x) = (\alpha_1 e^{\beta x} + \alpha_2 e^{-\beta x}) + c_{v,sat}, \tag{22}$$

where

$$\beta = \sqrt{\gamma / D_v^{sim}}. \quad (23)$$

(N_{mb}) and the anode channel condition using (11) and (12),

$$\begin{aligned} \alpha_1 e^{\beta L} + \alpha_2 e^{-\beta L} &= c_{v,an,ch} - c_{v,sat}, \\ \alpha_1 - \alpha_2 &= -N_{mb}/\beta D_v^{sim}. \end{aligned} \quad (24)$$

Determination of N_{mb} requires knowledge of the water vapor concentrations on both sides of the membrane ($x = 0$),

$$\begin{aligned} c_{v,an,mb} &= (\alpha_1 + \alpha_2) + c_{v,sat}, \\ c_{v,ca,mb} &= (\nu_1 + \nu_2) + c_{v,sat}. \end{aligned} \quad (25)$$

The ν_i for the cathode, similar to the α_i, are dependent upon N_{mb} and the cathode channel condition, but are additionally influenced by the water vapor reaction term $N_{v,rct}$,

$$\begin{aligned} \nu_1 e^{-\beta L} + \nu_2 e^{\beta L} &= c_{v,ca,ch} - c_{v,sat}, \\ \nu_1 - \nu_2 &= (-N_{mb} + N_{v,rct})/\beta D_v^{sim}, \end{aligned} \quad (26)$$

with $N_{rct,v} = \frac{I_{st}}{2F}$.

A. Liquid Water Governing Equation

Under the assumption that water vapor reaches quasi steady-state instantly, we replace the $c_{v,an}$ coupling term in (8) by its steady-state solution (22). The PDE for liquid water distribution in the porous medium is then,

$$\frac{\partial s}{\partial t} = \frac{\partial}{\partial x}\left(b_1 S^{b_2} \frac{\partial s}{\partial x}\right) + \frac{M_v \gamma}{\rho_l}(\alpha_1 e^{\beta x} + \alpha_2 e^{-\beta x}), \quad (27)$$

for $s \geq s_{im}$, and

$$\frac{\partial s}{\partial t} = \frac{M_v \gamma}{\rho_l}(\alpha_1 e^{\beta x} + \alpha_2 e^{-\beta x}), \quad (28)$$

for $0 < s < s_{im}$, where β and α_i are as defined in the $c_{v,an}(x,t)$ solution previously.

We define a Semi-Analytic Solution (SAS) that combines the analytic solutions for the gas constituents ($H_2, O_2, c_{v,an}, c_{v,ca}$) with the liquid water ratio ($s_{an}(x(k),t)$ and $s_{ca}(x(k),t)$) numeric DAE, where the k represents a counter for the discretized sections in the spatial variable, x. For analysis and comparison, we present with the SAS a 3-section Coarse Numeric Solution (CNS) version of the system with six 2^{nd} order GDL PDEs and five channel ODEs, as presented in [4].

V. Cell Voltage

The estimated cell voltage, $\hat{v}$, is equal to the theoretical open circuit voltage less the activation, ohmic, and concentration voltage losses,

$$\hat{v} = E - U_{act} - U_{ohmic} - U_{conc}. \quad (29)$$

Typical fuel cell operation avoids the concentration loss range of current density, therefore $U_{conc} = 0$. The theoretical open circuit voltage varies with temperature, reactant partial pressures, and temperature according to [10],

$$E = -\left(\frac{\Delta H}{2F} - \frac{T_{st}\Delta S}{2F}\right) + \frac{RT_{st}}{2F} \ln\left(\frac{p_{H_2,mb}\sqrt{p_{O_2,mb}}}{p_o^{1.5}}\right), \quad (30)$$

where ΔS and ΔH are the differences in entropy and enthalpy from standard conditions, p_o is the standard pressure, and $p_{O_2,mb}$ and $p_{H_2,mb}$ are taken from the GDL Section 1.

The activation voltage loss is modeled using,

$$U_{act} = K_1 \frac{RT_{st}}{F} \ln\left(\frac{i_{app} + i_{loss}}{i_o}\right), \quad (31)$$

where K_1 =1.00 is a charge transfer-related coefficient and i_{loss} is the loss current density due to H_2 crossover, and the exchange current density, i_o, is given by,

$$i_o = K_2 \left(\frac{p_{O_2,mb}}{p_o}\right)^{K_3} \exp\left[-\frac{E_c}{RT_{st}}\left(1 - \frac{T_{st}}{T_o}\right)\right], \quad (32)$$

where $K_2 = 1.24\ \mu A$ and $K_3 = 2.05$ are tunable parameters, E_c is the activation energy for oxygen reduction on Pt, and T_o is the reference temperature.

The ohmic voltage loss model is taken from [11], including the experimentally identified parameters b_{11} and b_{12}, and modified with the final tunable parameter $K_4 = 3.40$,

$$U_{ohmic} = K_4 \left[\frac{t_{mb}}{(b_{11}\lambda_{mb} - b_{12})} e^{-1268\left(\frac{1}{303} - \frac{1}{T_{st}}\right)}\right] i_{app}, \quad (33)$$

where t_{mb} is the membrane thickness, λ_{mb} is the membrane water content, and the apparent current density, i_{app}, is explained in V-A.

A. Apparent Current Density

The apparent active area A_{app} translates the mass of liquid water accumulated in the anode channel into an apparent current density,

$$i_{app} = \frac{I_{st}}{A_{app}}. \quad (34)$$

A_{app} is the cell total active area less the area occupied by the thin film of liquid water that is assumed to form on the GDL-channel interface,

$$A_{app} = A_{fc} - \frac{2m_{l,ch}}{\rho_l t_{wl}}. \quad (35)$$

The film thickness, $t_{wl} = 0.14$ mm is another tunable parameter, and includes the factor of 2 in the numerator since only half of the GDL-channel interfacial area is available for coverage due to the gas distributor land area.

The channel liquid water mass comes from the dynamic water mass balance in the channel (17), and is found by assuming that any water in the channel in excess of the maximum that can be held in vapor is in liquid form,

$$m_{l,ch} = max\left[0, m_{w,ch} - c_{v,sat} M_v V_{ch}\right]. \quad (36)$$

VI. Verification of the Semi-Analytic Model

The model predicts voltage degradation by establishing a causal relationship between anode channel flooding and the fuel cell voltage deterioration. The experiments were performed using a 24-cell stack with an active area of 300 cm^2. The experiment operated with a dead-ended anode, and

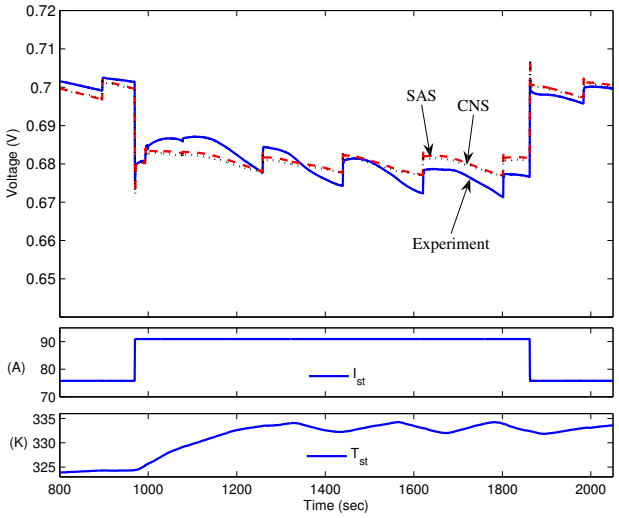

Fig. 3. The semi-analytic model is able to capture static and transient trends in a direct comparison to experimental voltage output. Further, the semi-analytic solution generates a voltage estimate very similar to the numeric solution (A_{fc}=300cm^2).

the necessary purges executed on 180 second intervals for a duration of 1 second. For further experiment details, readers are requested to see [4].

In the first verification experiment, the stack current was varied from 75A → 90A → 75A while temperature was thermostatically controlled from 50C → 60C. Comparing the numeric model to the semi-analytic model in Fig. 3 illustrates that little, if any, predictive accuracy has been lost by implementing the semi-analytic solution to the GDL dynamics, and the important trends related to transient manifold pressure dynamics and stack current changes are captured. A desirable

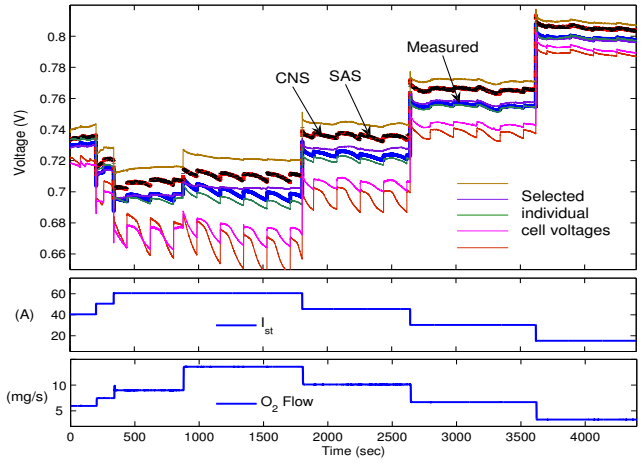

Fig. 4. The voltage prediction captures fluctuations due to changing conditions, and bias is within the cell-to-cell variation.

aspect of the model's control-oriented goal is estimation of the behavior of a 24-cell stack using a single cell model. In the set of experimental results shown in Fig. 4 a (200% → 300%) stoichiometry change is added to a series of stack current steps (40A → 60A → 15A). This data illustrates the range of voltage outputs from the individual cells in the stack. Though the model voltage prediction departs from the stack average value for some conditions, trends are still captured and the results are still within the range of individual cell values. The semi-analytic model output again tracks the numeric model closely.

VII. Investigation of Control Requirements

The semi-analytic model of the liquid water and water vapor distributions can be utilized to control channel flooding, and thus potentially avoid voltage output degradation due to excessive water in the cell. We can relate a measurable quantity, the channel relative humidity, with an unmeasurable state of interest, the GDL quantity of liquid water. Fig. 5 shows the steady-state solutions for water vapor concentration and liquid water fraction in the anode found using a simultaneous system solution process. This process uses cell inlet and outlet conditions, in addition to the stack temperature and stack current, and provides cathode and anode water vapor concentration distributions via analytic solution (22), using the model estimate of the membrane water transport (13). Figure 5 demonstrates that the steady-state solutions to the

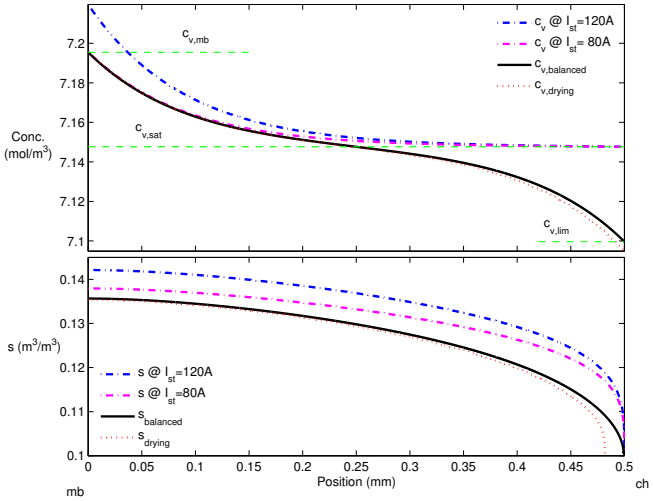

Fig. 5. Anode distribution of liquid water ratio for varying channel water vapor concentrations illustrates that the channel water vapor concentration boundary value can shape the liquid water distribution.

water PDEs lead to an exponential form for the vapor and a fractional power polynomial for the liquid. These shapes are highly dependent upon the choice of boundary conditions, as evidenced by results from [12], whose numeric results show much higher liquid ratios (s>0.80) at the membrane and zero liquid water at the channel, due to the assumptions of liquid water transport across the membrane and $s = 0$ at the GDL-channel interface. Recent results [13] support the membrane boundary condition (14) used here.

Liquid water in excess of the immobile saturation (i.e. flooding) exists in the GDL when the water vapor concentration exceeds $c_{v,sat}$ in the channel. At lower channel water vapor concentrations, we observe a channel condition for

which the GDL two-phase boundary begins to recede into the GDL. The channel water vapor concentration for this condition is $c_{v,an,ch} = 2c_{v,sat} - c_{v,mb} \triangleq c_{v,lim}$.

We postulate that if $c_{v,an,ch}$ can be controlled such that it equals $c_{v,lim}$, then the flow into the GDL (from membrane water transport) will equal the flow out of the GDL (into the channel), and hence this condition represents a potential equilibrium point for zero liquid build-up in the channel while maintaining the membrane humidification at its highest possible value. If the value of $c_{v,an,ch}$ falls below $c_{v,lim}$, then the water two-phase front will recede into the GDL, and cause an abrupt, and easily detectable, channel water vapor concentration change due to the depletion of liquid water and subsequent loss of its associated evaporation contribution.

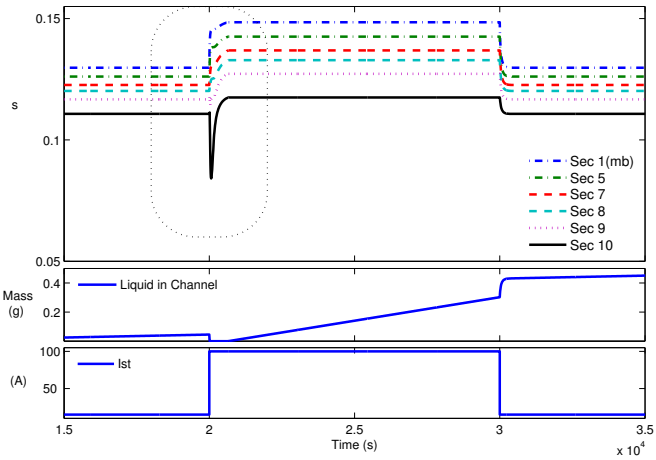

Fig. 6. Simulation result for a set of conditions that results in eventual channel flooding. A step in load at t=20000 s brings the channel into high flooding condition, and a step down returns to the previous liquid distribution in the GDL, but the channel water mass continues to grow.

Figure 6 demonstrates the response of the semi-analytic model, discretized into 10 sections for illustrative purposes, to load (current) step changes up and back down to the original level. At time t=20000s, an 80A step increase in I_{st} is applied as shown in the dotted box, demonstrating how stack current variation causes competing responses between GDL areas near the membrane and those near the channel. On the membrane side, the increase in load causes a proportional increase in generated water which results in a higher value of $s(1)$. This effect ripples through the GDL as a higher s equilibrium value is reached for each section. From the channel side, the increased current demand is fed forward to the reactant supply, which increases H_2 inflow to maintain stoichiometry. The higher volumetric flow rate removes more water from the anode channel, resulting in greater evaporation and a dip in $s(10)$ near the channel. These competing phenomena meet and the increase in water generated overcomes the greater water removal and pushes the GDL to overflow into the channel, causing the flooding displayed by the increasing slope of the channel liquid fraction. The I_{st} step-down at t=30000s returns the GDL liquid water distribution to its previous level, lowering the rate of liquid flow into the channel, but the channel liquid water mass is greater than before the step, and voltage degradation is predicted.

VIII. Conclusions and Future Work

A first principles semi-analytic model describing the reactant, water vapor, and liquid water dynamics in a polymer electrolyte membrane fuel cell has been verified by voltage output comparison. Additionally, a method to simultaneously obtain the water vapor concentration analytic solutions across the membrane is provided so that solutions can be obtained using only physically available system inputs and outputs.

The semi-analytic model enables fast and computationally inexpensive estimation of GDL states. Required steps to simulate, CPU time, and function calls all decreased significantly ($\sim$40%) compared to the equivalent numeric model.

Future work will use the results presented to establish cell voltage and channel humidity feedback-based control algorithms to shape the liquid water distribution indirectly via control of the water vapor channel concentration. The proposed channel water vapor concentration ($c_{v,lim}$), has potential to eliminate channel flooding while maximizing membrane water content under the zero channel liquid constraint. Prior to implementation of control, however, stability and controllability/observability analysis must be completed.

References

[1] K. Promislow and J. Stockie, "Adiabatic relaxation of convective-diffusive gas transport in a porous fuel cell electrode," *SIAM J. Appl. Math.*, vol. 62, pp. 180–205, 2001.

[2] A. Shah, G. Kim, W. Gervais, A. Young, K. Promislow, and D. Harvey, "The effects of water and microstructure on the performance of polymer electrolyte fuel cells," *J. Power Sources*, pp. 1251–1268, 2006.

[3] H. Yamada and Y. Morimoto, "Practical approach to polymer electrolyte fuel cell modeling," vol. 39, 2004.

[4] D. A. McKay, J. B. Siegel, W. T. Ott, and A. G. Stefanopoulou, "Parameterization and prediction of temporal fuel cell voltage behavior during flooding and drying conditions," *J. Power Sources*, vol. 178, no. 1, pp. 207–222, 2008.

[5] J. H. Nam and M. Kaviany, "Effective diffusivity and water-saturation distribution in single- and two-layer PEMFC diffusion medium," *Int. J Heat Mass Transfer*, vol. 46, pp. 4595–4611, 2003.

[6] D. McKay, J. Siegel, W. Ott, and A. Stefanopoulou, "Parameterization and prediction of temporal fuel cell voltage behavior during flooding and drying conditions," *Submitted to J. Power Sources*, 2007.

[7] H. Meng and C.-Y. Wang, "Electron transport in PEFCs," *J. Electrochem. Soc.*, pp. A358–A367, 2004.

[8] N. Siegel, M. Ellis, D. Nelson, and M. von Spakovsky, "A two-dimensional computational model of a PEMFC with liquid water transport," *J. Power Sources*, pp. 173–184, 2006.

[9] B. A. McCain, A. G. Stefanopoulou, and I. V. Kolmanovsky, "A multi-component spatially-distributed model of two-phase flow for estimation and control of fuel cell water dynamics." New Orleans, LA, USA: IEEE Conference on Decision and Control, December 2007, CDC2007-1455.

[10] R. O'Hayre, S. Cha, W. Colella, and F. Prinz, *Fuel Cell Fundamentals*. Hoboken: Wiley, 2006.

[11] T. Springer, T. Zawodzinski, and S. Gottesfeld, "Polymer electrolyte fuel cell model," *Journal of the Electrochemical Society*, 1991.

[12] D. Natarajan and T. Nguyen, "A two-dimensional, two-phase, multicomponent, transient model for the cathode of a proton exchange membrane fuel cell using conventional gas distributors," *J. Electrochemical Society*, pp. A1324–A1335, 2001.

[13] J. Owejan, J. Owejan, T. Tighe, W. Gu, and M. Mathias, "Investigation of fundamental transport mechanism of product water from cathode catalyst layer in PEMFCs." San Diego, CA, USA: 5th Joint ASME/JSME Fluids Engineering Conference, July 2007.